Direct Visualization of Lipid Domains in Human Skin Stratum Corneum's Lipid Membranes: Effect of pH and Temperature

I. Plasencia,* L. Norlén,† and L. A. Bagatolli*

*Membrane Biophysics and Biophotonics Group, Department of Biochemistry and Molecular Biology/MEMPHYS Center, University of Southern Denmark, Campusvej 55, DK-5230 Odense M, Denmark; and †Medical Nobel Institute, Departments of Cellular and Molecular Biology, Karolinska Institute, and Dermatology Clinic, Karolinska University Hospital, Stockholm, Sweden

ABSTRACT The main function of skin is to serve as a physical barrier between the body and the environment. This barrier capacity is in turn a function of the physical state and structural organization of the stratum corneum extracellular lipid matrix. This lipid matrix is essentially composed of very long chain saturated ceramides, cholesterol, and free fatty acids. Three unsolved key questions are i), whether the stratum corneum extracellular lipid matrix is constituted by a single gel phase or by coexisting crystalline (solid) domains; ii), whether a separate liquid crystalline phase is present; and iii), whether pH has a direct effect on the lipid matrix phase behavior. In this work the lateral structure of membranes composed of lipids extracted from human skin stratum corneum was studied in a broad temperature range (10°C–90°C) using different techniques such as differential scanning calorimetry, fluorescence spectroscopy, and two-photon excitation and laser scanning confocal fluorescence microscopy. Here we show that hydrated bilayers of human skin stratum corneum lipids express a giant sponge-like morphology with dimensions corresponding to the global three-dimensional morphology of the stratum corneum extracellular space. These structures can be directly visualized using the aforementioned fluorescence microscopy techniques. At skin physiological temperatures (28°C–32°C), the phase state of these hydrated bilayers correspond microscopically (radial resolution limit 300 nm) to a single gel phase at pH 7, coexistence of different gel phases between pH 5 and 6, and no fluid phase at any pH. This observation suggests that the local pH in the stratum corneum may control the physical properties of the extracellular lipid matrix by regulating membrane lateral structure and stability.

INTRODUCTION

The main function of the skin is to serve as a physical barrier at the interface between the body and the environment. This barrier capacity is largely a function of the physical state and structural organization of the extracellular lipid matrix of stratum corneum (1–4). Several models for the structural organization of the lipid matrix have been proposed, e.g., the domain mosaic model (2), the laminglass model of Pascher (cf. (5)), the sandwich model (6), the single gel phase model (4), and the asymmetric bilayer model (7). The main unsolved problems with respect to skin barrier lateral lipid organization (2,4,8–10) are i), whether the extracellular lipid matrix is constituted by a single gel phase or if there is a coexistence of several crystalline (solid) and/or gel phases; ii), whether a separate fluid phase is present; and iii), whether pH has a direct effect on the skin lipid phase behavior.

Stratum corneum lipid composition

Most published accounts of the human stratum corneum lipid composition have been complicated by the presence of sebaceous lipids and other exogenous contaminants. When stratum corneum samples are obtained from excised skin for lipid analysis, there is almost always massive contamination with triglycerides from subcutaneous fat. Furthermore, the human skin surface is coated with sebaceous lipids (11). This is a major source of squalene, wax esters, and triglycerides, which undergo hydrolysis to yield free fatty acids (FFAs) through the action of lipases present on the skin surface. The sebaceous fatty acids are mostly 16 and 18 carbons in length and contain high proportions of monounsaturated species and variable proportions of branched chains. This is in contrast to the stratum corneum fatty acids, which are longer than 20 carbons, saturated, and straight chained (12–14).

Until recently, skin ceramide analysis relied on gas chromatography/mass spectrometry (MS), necessitating ceramide hydrolysis, derivatization, and subsequent separate analysis of the resulting sphingoid bases and fatty acids, with consequent increased risks for lipid contamination. The introduction of electrospray ionization-mass spectrometry (ESI-MS) in the late 1980s allowed for direct detection of stratum corneum ceramide species, thereby avoiding most contamination sources. ESI-MS analysis has shown that ω-esterified human skin ceramides (named EOS, EOP, and EOH) contain amide-bound saturated fatty acids with chain lengths between 28 and 36 carbons peaking at 32–34 carbons and that remaining ceramides (named NS, NdS, NP, NH, AS, AP, and AH) have chain lengths between 20 and 36 carbons peaking at 26–28 carbons (15,16). The only ceramide species with reported medium chain lengths (C15–C18) is ceramide AS (15). However, this conflicts with the

Submitted August 28, 2006, and accepted for publication June 25, 2007.

Address reprint requests to Luis A. Bagatolli, MEMPHYS—Center for Biomembrane Physics, Dept. of Biochemistry and Molecular Biology, Campusvej 55, DK-5230 Odense M, Denmark. Tel.: 45-65-50-34-76; Fax: 45-65-50-40-48; E-mail: bagatolli@memphys.sdu.dk.

Editor: Thomas J. McIntosh.

0006-3495/07/11/3142/14 $2.00

doi: 10.1529/biophysj.106.096164

results of Vietzke et al. (16), who reported chain lengths between C22 and C36 for ceramide AS. In the stratum corneum extracellular space the relative amount of ceramides is ~50 wt %, cholesterol 35 wt %, and FFAs 15 wt % in an ~1:0.9:0.4 mol ratio (12–14,17).

Coexistence of crystalline and gel phases

In wide-angle x-ray diffraction (WAXD) experiments, the most frequently reported findings in isolated stratum corneum at skin physiological temperatures (28°C–32°C) are one sharp line at 3.7–3.8 Å, one sharp line at 4.1–4.2 Å, and one broad diffuse line at ~4.6 Å (18–24). At 40°C the 3.7–3.8 Å line is absent. This has been interpreted as a possible coexistence of crystalline (solid) lipid domains with hexagonal and orthorhombic hydrocarbon chain packing as well as with liquid crystalline (fluid) lipid domains. The coexistence of orthorhombic and hexagonal chain-packing lattices has also been supported by electron diffraction studies (25). A major problem with x-ray patterns of isolated stratum corneum is, however, the reported large variability of the obtained patterns between different samples, which is particularly striking for the lipid component (19). Further, most crystallographic data are derived from isolated stratum corneum that has been dehydrated during sample preparation and handling. It is far from evident that a dehydration-induced change of the stratum corneum lipid organization (e.g., a dehydration-induced hexagonal to orthorhombic transition) is reversible.

This is especially so as the lipid matrix exists under nonequilibrium conditions in vivo, exemplified by a strong gradient in water chemical potential present over the stratum corneum (9). Another example of a possible dehydration-induced artifact is the reported lipid-derived 13 nm lamellar repeat distance reported in some small-angle x-ray diffraction (SAXD) studies (23,26) and in conventional transmission electron microscopy studies of dehydrated epidermis (27). This 13 nm lamellar repeat distance has not been confirmed in other SAXD studies (19), in cryotransmission electron microscopy studies of native hydrated epidermis (28), or in neutron diffraction studies of hydrated stratum corneum (29). The observation that the 3.8 Å diffraction line disappears at ~40°C has been interpreted as a transition from an orthorhombic to a hexagonal chain-packing lattice (18). Isolated stratum corneum is, however, almost always contaminated by huge amounts of triacylglycerols originating from sebaceous glands and/or the subcutaneous fat (12–14,17).

An alternative interpretation is therefore that the disappearance of the 3.8 Å diffraction line at ~40°C represents the melting of contaminating crystalline medium chain lipids with orthorhombic chain packing. This is not unlikely as orthorhombic chain-packing lattices may melt directly into the liquid state when heated (for fat, the melting point of orthorhombic chain-packing lattices is higher than that of corresponding hexagonal lattices) and not via a hexagonal chain-packing lattice (30,31). In fact, this phenomenon is taken advantage of by the food industry in today's standard procedure for butter churning (''The Alnarp process'') (31). There is consequently no consensus on whether the stratum corneum extracellular lipid matrix is constituted by several coexisting crystalline (solid) phases or by a single gel phase.

Presence of a separate fluid phase

The presence of a fluid (or liquid crystalline) phase in the stratum corneum extracellular lipid matrix would have pronounced consequences for the barrier capacity of skin, as fluid membranes generally are 2–3 orders of magnitude more permeable to water than crystalline (solid) membranes (32). Further, fluid lipid crystals could allow formation of structures other than flat bilayers (L_α), such as oilcontinuous or bicontinuous morphologies (e.g., H_{II}, L_2, or V_2) (31). The formation of bicontinuous fluid lipid crystals could thus result in a direct penetration pathway for both hydrophilic and lipophilic substances through the stratum corneum, with dramatic consequences for skin permeability. The notion of the presence of a separate fluid phase in the stratum corneum extracellular space stems from the WAXD evidence in isolated stratum corneum, at physiological temperatures, of a broad diffuse line at ~4.6 Å (18,21,23,24), and from the evidence of a fluid signal in in vivo attenuated total reflectance-infrared (ATR-IR) spectroscopy assessments of stripped stratum corneum (33). However, lipid hydrocarbon chain ends of gel phases are supposed to be disordered. Even for pure orthorhombic lipid crystals the 2–6 lowermost carbons usually show liquid-like disordering (I. Pascher, Göteberg University, personal communication, 2002). Also, both the fluid ATR-IR signal and WAXD ~4.6 Å broad diffuse line may predominantly have been derived from lipids of sebaceous origin (33). There is consequently no consensus on whether a separate fluid phase is present in the stratum corneum extracellular lipid matrix.

Effect of pH on skin barrier function

Stratum corneum pH is believed to be of central importance for skin barrier capacity (34–38). Skin diseases characterized by a perturbed skin barrier function, such as atopic dermatitis, irritant contact dermatitis, and ichthyosis vulgaris, express an elevated skin surface pH (39–42). However, the pH gradient over the stratum corneum, which is more relevant for the extracellular lipid matrix and thus for skin barrier function, is normal in ichthyosis vulgaris (40). Similar data for atopic dermatitis and irritant contact dermatitis are lacking. Also, newborn infants express an elevated skin surface pH for several weeks postnatally, whereas skin barrier function physically is normal (43). On the other hand, newborn infants show an increased susceptibility to develop irritant contact dermatitis, suggesting an impaired skin barrier function (44). Sustained elevation of stratum corneum pH by

topically applied tetramethylguanidine dissolved in propylene glycol/ethanol has been claimed to decrease skin barrier capacity as measured by an increased transepidermal water loss (TEWL) (38). TEWL measures the difference in vapor pressure at two points situated on a line perpendicular to the skin surface inside a tunnel pressed toward the skin (45). In the absence of skin irritation, TEWL may be considered an indirect measure of stratum corneum water permeability (46).

Effect of pH on stratum corneum lipid phase behavior

The bulk pH of the stratum corneum and upper viable epidermis has been measured to 4.0–4.5 (47) and to 5.0–7.0 (48), respectively, and the local pH of the stratum corneum extracellular lipid matrix (in mice) to ~6 (49).

Langmuir-Blodgett films of extracted human skin stratum corneum extracellular lipids composed of purified ceramides, cholesterol, and FFAs do not show a dependence on subphase pH between pH 3 and 8, as observed by atomic force microscopy (AFM) (10). This is surprising as the ionization state of the FFA palmitic acid (C16:0) modulates its interaction with cholesterol (50). Speculatively, the rigid gel state organization of the skin lipid model systems may have diminished the effect of pH on lateral lipid organization in the AFM experiments. Also, a structuring effect exerted by the substrate (mica) surface cannot be excluded (51). X-ray diffraction studies of isolated ceramides, cholesterol, and FFAs have reported a pH dependence on the lamellar lipid organization but not on the lateral lipid organization (52). There is consequently no consensus on whether pH has a direct effect on skin barrier lipid lateral organization.

Lateral lipid organization of hydrated bilayers of extracted skin stratum corneum lipids

In this work we directly visualize the lateral structure of membranes composed of lipids extracted from skin stratum corneum at different temperatures (including skin physiological temperature) using two photon excitation and confocal fluorescence microscopy by means of different fluorescence probes (such as Laurdan, whose emission is sensitive to the lipid lateral organization (53)). Our microscopy results are complemented with other experimental techniques such as differential scanning calorimetry (DSC) and fluorescence spectroscopy. Giant lipid structures with sizes on the order of tens of micrometers are generated to directly observe and characterize the microscopic scenario of these particular membranes. Interestingly, these structures have dimensions corresponding to the global three-dimensional (3D) morphology of the stratum corneum extracellular space. Here we show that at skin physiological temperatures, the phase state of these hydrated bilayers correspond microscopically (radial resolution limit 300 nm) to i), a single gel phase at pH 7; ii), a coexistence of different gel (or solid) phases between pH 5 and 6 (characterized by presence of micron-sized lipid domains); and iii), no fluid phase at any pH. This observation suggests that the local pH in the stratum corneum may control the physical properties of the extracellular lipid matrix by regulating membrane lateral structure and stability. Finally, we show that the lateral organization of membranes composed of extracted stratum corneum lipids differs from that of canonical commercial lipid mixtures. We particularly emphasize the importance of the visual information provided by fluorescence microscopy techniques when compositionally complex lipid mixtures are compared.

MATERIALS AND METHODS

Materials

1,1′-Dioctadecyl-3,3,3′,3′-tetramethylindocarbocyanine perchlorate (DiI_{C18}) and 6-lauroyl-2-(*N*,*N*-dimethylamino)naphthalene (Laurdan) were purchased from Molecular Probes (Invitrogen, Copenhagen, Denmark). Bovine brain ceramide and cholesterol were from Avanti Polar Lipids (Alabaster, AL). Fatty acids were purchased from Sigma-Aldrich (Copenhagen, Denmark). The natural skin mixture used in our experiments was prepared using the ceramide and cholesterol fraction extracted from human stratum corneum lipid ($_{HSC}$(Cer/Chol)) (12–14,17) and supplemented with commercial FFAs (5:11:39:23:8:2 mol of C20:0, C22:0, C24:0, C26:0, C28:0, C30:0, corresponding to the natural distribution of the FFA component of the lipid matrix of the stratum corneum extracellular space (12)). The final mixture keeps the previously reported natural molar ratio $_{HSC}$(Cer/Chol)/FFA 1:0.9:0.4 (17). Lipid mixtures from five different individuals were used in our experiments. At least two of these five different mixtures were randomly used in each different set of experiments. No significant differences in the obtained data were observed among these samples.

Methods

Differential scanning calorimetry

Lipid stock solutions were prepared in $CHCl_3$ at 2.2 mg/mL assuming for ceramides a molecular weight average of 566. A proper amount of lipids were transferred to a glass tube, and the organic solvent was removed under a stream of N_2. The sample (see Table 1) was placed overnight under vacuum to remove traces of organic solvents. The dried lipid mixtures were hydrated using MilliQ water (Millipore, Bedford, MA) (pH ~5.7) in a thermomixer (Eppendorf Nordic, Horsholm, Denmark) by heating and vortexing continuously for 30 min until turbid lipid suspensions were observed (final lipid concentration 5 mM). Subsequently the samples were passed through four freezing-thawing cycles (−80°C and 90°C, respectively). These cycles were repeated until the suspension was totally homogeneous. The sample was loaded in a Science Corp (Lindon, UT). N-DSCII microcalorimeter and equilibrated for 10 min. Four scans, each corresponding to one heating and one cooling cycle, were collected from each sample between 10°C and 95°C,

TABLE 1 Sample composition used in this study

Sample	Mol ratio
bbCer/Chol/LA	1:1:1
$_{HSC}$(Cer/Chol)/FFA	1:0.9:0.4

Abbreviations: bbCer, bovine brain ceramide; Chol, cholesterol; LA, lignoceric acid; $_{HSC}$(Cer/Chol), ceramide and cholesterol fraction extracted from human stratum corneum (keeping the native ratio); FFA, free fatty acid keeping the natural composition (C20:0; C22:0; C24:0; C26:0; C28:0; C30:0) and molar ratio (5; 11; 39; 23; 8; 2, mol ratio).

at a rate of 0.5°C/min. No differences were observed after the four temperature cycles. The data were processed with Origin v7.0383 (Northampton, MA).

Laurdan GP measurements

A stock solution of Laurdan was made in methanol. Lipid stock solutions were prepared in $CHCl_3$. Lipid-probe dispersions were prepared using a lipid/probe ratio of 400:1 (Laurdan final concentration was 1 μM). The dried lipid mixtures were hydrated with MilliQ water (pH $\sim$ 5.7) or with the corresponding buffer depending on the desired pH (pH = 5–6 MES (2-(*N*-morpholino)-ethanesulphonic acid) 0.5 mM; pH = 7–8.2 buffer HEPES 0.5 mM; pH = 11 buffer CAPS (3-(cyclohexylamino)-propanesulfonic acid) 0.5 mM) using the same procedure described for the DSC experiment. All samples were prepared and stored in the dark, and the emission spectra were measured immediately after preparation. The Laurdan generalized polarization (GP) denotes the position of the probe's emission spectra (54). The fluorescence emission properties of Laurdan are sensitive to the water dipolar relaxation process that occurs in the probe's local environment (the lipid bilayer in this case). The extent of water dipolar relaxation observed in the gel phase is very low compared to that observed in the fluid phase. As a consequence the probe's emission is blue in the gel phase and green in the fluid phase (54). The GP function was defined analogously to the fluorescence polarization function as:

$$\mathrm{GP} = \frac{I_\mathrm{B} - I_\mathrm{R}}{I_\mathrm{B} + I_\mathrm{R}}, \qquad (1)$$

where I_B and I_R correspond to the intensities at the blue and red regions of the emission spectrum, respectively, using a given excitation wavelength (54). Consequently, the Laurdan GP is related to the lateral packing of the lipid bilayers (54). High Laurdan GP values (0.4–0.6) correspond to laterally ordered phases (gel-like), whereas low Laurdan GP values (below 0.2) correspond to fluid phases. To measure the GP of the Laurdan-labeled multilamellar vesicles, a Chronos ISS fluorometer (ISS, Champaign, IL) was used. The excitation wavelength was 374 nm (using a laser diode as excitation source). The emission wavelengths were 440 nm for the I_B and 490 nm for the I_R (Eq. 1).

Fluorescence microscopy

Lipids stock solutions in $CHCl_3$ (1 mg/mL) were premixed with the fluorescent probe (DiI_{C18} or Laurdan 0.5 mol %). An aliquot (50 μL) of the lipid stock solution was spread on a rectangular glass coverslip coated with a thin ITO layer (Indium Tin Oxide, ITO electrode). After this procedure the ITO electrode was placed under vacuum overnight. The crystal then was inserted in a homemade electroformation chamber (previously described (55)) and filled with MilliQ water. The electroformation procedure consists of application of an alternate field (amplitude 4 V, frequency 10 Hz) using a function generator (Digimess Fg 100, Fürth, Germany) between the two ITO electrodes (one containing the lipid sample) during 45 min at 80°C.

The membrane structures obtained were observed at the desired temperature in the abovementioned electroformation chamber using a Zeiss-LSM 510 META NLO inverted microscope (Zeiss, Jena, Germany) using a 20× air objective (numerical aperture 0.75). For the two-photon excitation mode this microscope is coupled with a titanium:sapphire laser (Broadband Mai Tai XF-W2S with 10 W Millennia pump laser, tunable excitation range 710–980 nm; Spectra Physics, Mountain View, CA). The excitation wavelengths in our experiments were 543 nm (for DiI_{C18} in one-photon excitation mode) and 780 nm (for Laurdan in two-photon excitation mode). The fluorescence signals were collected in different channels using band-pass filters of 590 $\pm$ 26 nm for DiIC18 and 424 $\pm$ 37 nm and 525 $\pm$ 25 nm for Laurdan. The two-photon excitation Laurdan GP images were computed using the fluorescence images obtained with the aforementioned band-pass filters using a routine included in the Flim-FCS program Global for images (LFD, Irvine, CA).

3D image projections presented in Figs. 2, 5, and 6 were constructed with the commercial software from Zeiss. Stack series of 50–200 images (depending on the height of the sponge-like structure) were acquired with an image separation of 500 nm, corresponding to axial distances between 25 and 100 μm. When visualization was done at the level of single-lipid structures (either giant vesicles or sponge-like structures), the general behavior was recorded on multiple lipid structures. All fluorescent images shown in Figs. 2, 5, and 6 are representative of at least 20 sponge-like structures. The same approach was used for the GP analysis (see above).

The GP histogram analysis was performed using SimFCS software (i.e., the same software used to calculate the GP images, see above). Each GP histogram in Fig. 3 represents the GP value pixel distribution (one GP value per pixel) obtained from an isolated region corresponding to a single lipid phase. The average GP value, obtained from the center values of multiple GP histograms, was calculated for each lipid phase. At least eight different regions of the same lipid phase were chosen for every GP image, and at least four images were obtained for every temperature. The GP histograms for individual regions were then calculated, and the average GP values used to generate the diagram in Fig. 4.

The pH effect has been observed in two different ways. Either the samples were prepared at a desired pH (5, 7, or 8) or the samples were prepared at pH 5 and then the original buffer solution was exchanged with other buffers (pH = 5–6 MES 0.5 mM; pH = 7–8.2 buffer HEPES 0.5 mM; pH = 11 buffer CAPS 0.5 mM) using a special device included in the homemade chamber. The local pH in these experiments was checked with a 744 Metohm pHmeter (Bie&Berentsen, Copenhagen, Denmark). All measurements were repeated at least twice. No measurable differences were observed among the samples obtained from different individuals.

RESULTS

Thermotropic characterization of the $_{HSC}$(Cer/Chol)/FFA mixture

DSC and Laurdan GP cuvette experiments

Fig. 1 shows the DSC data obtained with the $_{HSC}$(Cer/Chol)/FFA lipid mixture. The mixture displays a broad thermogram characterized by two main phase transitions at 35°C and 69°C (see Table 2). This corresponds well to the thermotropic transitions attributed to the stratum corneum lipid components reported in the literature (56,57). The low melting phase transition observed at 35°C has not previously been recorded in stratum corneum lipid extracts but only in native stratum corneum (56–59).

Fig. 1 further shows the Laurdan GP temperature profile of multilamellar vesicles composed of $_{HSC}$(Cer/Chol)/FFA. Laurdan GP shows a main event around 65°C, indicating a change in the extent of water dipolar relaxation around the probe. This event corresponds to a lipid phase transition correlating with the high melting phase transition observed in the DSC experiment (Fig. 1). This transition is likely for the gel/fluid-disordered type because of the observed GP values (54,60). On the other hand, the Laurdan GP profile did not show a change corresponding to the phase transition event at 35°C observed by DSC. Based on the GP values (54) we conclude that below 40°C this membrane shows the presence of a gel-like (or solid) phase.

The complexity of the lipid composition and the lack of knowledge of the thermotropic behavior of the individual components (in particular the ceramide species) make it

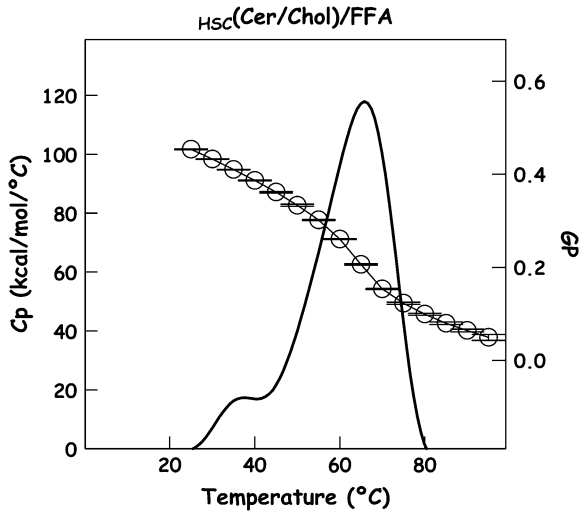

FIGURE 1 DSC experiments and Laurdan GP temperature profile of $_{HSC}$(Cer/Chol)/FFA mixture (1:0.9:0.4 mol). The DSC temperature scans were collected from each sample between 10°C and 95°C, at a rate of 0.5°C/min. The GP values observed at the low temperature regime (below 40°C) indicate that the membrane is in a gel- (or solid)-like phase state (see text). For all samples two independent batches were used for the experiments. Four DSC scans and five GP measurements per temperature were performed per batch.

difficult to identify the specific molecular species participating in the observed phase transitions. For simple mixtures this information is essential to assign potential lipid phases, including phase coexistence phenomena. It was consequently difficult to obtain a more detailed picture of the lipid phase scenario in our complex mixture. Even though the obtained DSC and fluorescence spectroscopy (GP) data yield coarse information of the physical properties of our complex system, more information is needed for a complete description of its lipid phase scenario.

Fluorescence microscopy experiments

One way to directly observe the lateral lipid structure is by fluorescence microscopy (61,62). It further allows membrane morphology to be directly coupled with molecular level dynamical and structural information obtained by fluorescence spectroscopy. Fluorescence microscopy of giant lipid structures can yield detailed information about the lateral structure of different lipid mixtures, including membranes composed of native material (55,63). Fig. 2 shows fluorescent images of DiI_{C18} labeled giant lipid structures composed of the $_{HSC}$(Cer/Chol)/FFA mixture prepared by the electroformation method (see Materials and Methods section). The giant lipid structures express a sponge-like morphology and differ from the multiple isolated giant unilamellar vesicles (GUVs) observed with phospholipid-containing mixtures. The observed sponge-like structures consist of ''columns'' of aggregated giant lipid vesicles. Several of these columns are formed on the surface of the ITO electrode, and isolated GUVs are very scarce. The generation of the sponge-like structure is independent of the lipid concentration used (data not shown). Additional analysis of fluorescence intensity was done in different cross sections of the sponge-like structure to check the lamellarity of the membranes. The fluorescence intensity was measured in the isolated membranes and at the point of contact among the vesicles. By dividing the intensity of the isolated membranes by that measured in the contact points, discrete numbers are obtained. These numbers are related with the lamellarity of the membrane (64). The computed number of lamellas of the sponge-like structure corresponded to 1.0 ± 0.4 (mean ± SD, $n = 10$) and 2.1 ± 0.4 (mean ± SD, $n = 10$) for the isolated membranes and the contact areas, respectively. This suggests the presence of unilamellar membranes in the sponge-like structure.

TABLE 2 Tm and ΔH values from the DSC thermograms

Sample	Tm_1 (°C)	Tm_2 (°C)	ΔH_1 (kCal/mol)	ΔH_2 (kCal/mol)
bbCer/Chol/LA	52	72	1.5	1.5
$_{HSC}$(Cer/Chol)/FFA	35	69	0.24	1.02

Abbreviations: bbCer, bovine brain ceramide; Chol, cholesterol; LA, lignoceric acid; $_{HSC}$(Cer/Chol), ceramide and cholesterol fraction extracted from human stratum corneum (keeping the native ratio); FFA, free fatty acid keeping the natural composition (C20:0; C22:0; C24:0; C26:0; C28:0; C30:0) and molar ratio (5; 11; 39; 23; 8; 2, mol ratio).

A main change in the lateral structure of $_{HSC}$(Cer/Chol)/FFA membranes was observed at ~70°C using fluorescence microscopy. This is reflected by the homogeneous distribution of the fluorescence probe in the membrane above 70°C, followed by the presence of dark areas (domains) coexisting with fluorescent areas as the temperature is decreased below 70°C (Fig. 2 *B*). This transition temperature agrees with that observed by DSC and Laurdan GP in cuvettes. The presence of lipid domains observed with $DiIC_{18}$ persists down to 20°C (the lowest temperature used in the microscope experiments), i.e., at temperatures where DSC shows the second phase transition event. The dark micron-sized lipid domains observed at and below 35°C have an elongated dendritic-like shape with an average width of ~1 μm. These domains are interconnected, showing a percolation pattern (Fig. 2 *B*). Further, as the observed domains are not fluorescent and the probe distributes equally in both bilayer's leaflets, the lipid domains must span the bilayer (intrabilayer coupling). This is in agreement with that reported for GUVs composed of lipid mixtures of different compositional complexity (55,62,63,65–67) and also supports the idea that unilamellar structures are present in the sponge-like structure. Domain interbilayer coupling is very unlike and has so far not been observed in giant multilamellar vesicles (61).

The information obtained with $DiIC_{18}$ defines the lipid domain shape and size but does not provide information about the domain phase state. To obtain information about the phase state of the coexisting domains, Laurdan GP images were recorded at different temperatures (Fig. 3). Above 70°C, Laurdan shows a homogeneous distribution in the membrane, which is in agreement with that observed

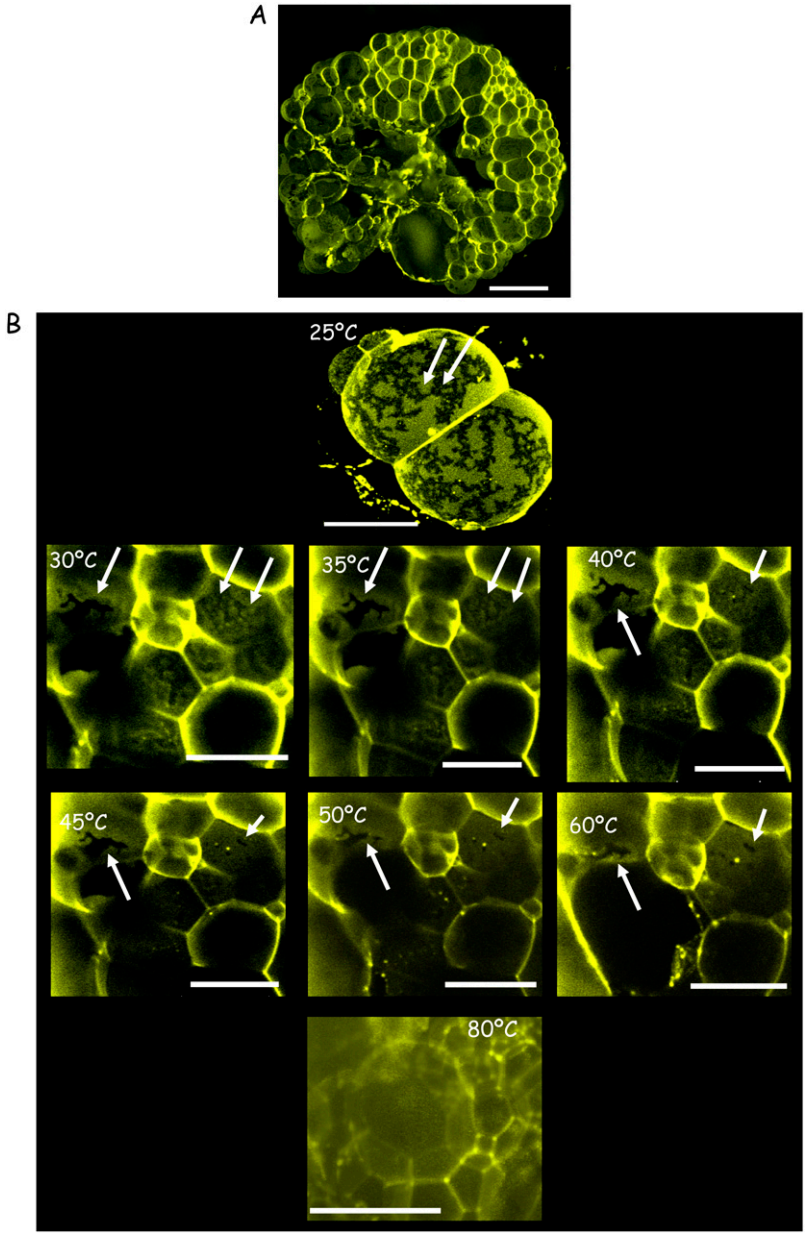

FIGURE 2 Confocal fluorescence 3D images (false color representation) of the $_{HSC}$(Cer/Chol)/FFA. (*A*) Sponge-like structure formed for the $_{HSC}$(Cer/Chol)/FFA lipid mixture after electroformation. Bar is 50 μm. (*B*) Effect of temperature on the $_{HSC}$(Cer/Chol)/FFA giant lipid structures. The images show the observed phase scenario for the skin lipids in MilliQ water (pH ~5.7) at different temperatures. Bars are 20 μm. Lipid domains are observed below 70°C (*arrows*). The fluorescent probe used was DiI_{C18}. All measurements have been repeated at least twice from three independent preparations.

with $DiIC_{18}$. The computed GP value of ~0.1 corresponds to a fluid-disordered-like phase. Between 40°C and 70°C the images show two different GP areas (~0.4 and ~0.1), indicating coexistence of fluid-disordered and gel-like lipid phases. A correlation can be established between the $DiIC_{18}$ and Laurdan data in this temperature regime, i.e., the dark domains shown in Fig. 2 *B*, using the probe $DiIC_{18}$ corresponding to gel phase domains.

Below 40°C Laurdan detects a change in the lateral distribution of the sample. This change is characterized by the observation of a homogeneous phase with GP values above 0.42, instead of the gel/fluid-disordered-like phase coexistence pattern observed between 40°C and 70°C. The Laurdan GP images observed below 40°C also show a strong photoselection effect. This last effect (together with the high Laurdan GP values) suggests that the lipid organization below 40°C may correspond either to gel or solid lipid phases, precluding the presence of fluid phases (because the photoselection effect is highly diminished; see Discussion and Conclusions section). Further, the temperature range where the change in the Laurdan GP images was observed (below 40°C) was in accordance with the low temperature thermal event detected by DSC (see Fig. 1).

The fact that $DiIC_{18}$ show lipid domain coexistence below 40°C may seem contradicted by the Laurdan GP images (Fig. 3) observed in the same temperature range. However, it is important to remark that if different ordered phases (gel- or solid-like phases, for example) are present, one does not

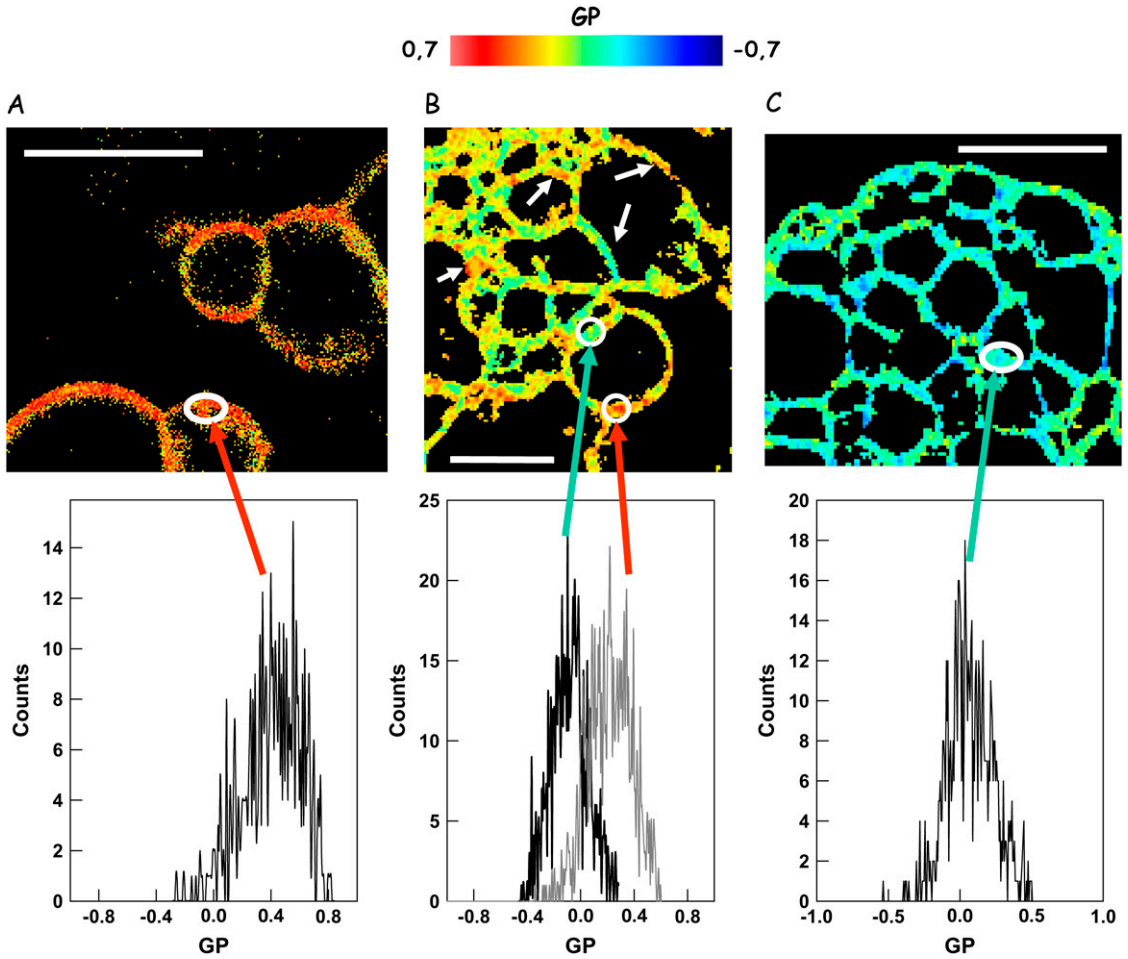

FIGURE 3 Laurdan GP images and Laurdan GP histograms of membranes composed of $_{HSC}$(Cer/Chol)/FFA (1:0.9:0.4) at three different temperatures in MilliQ water (pH ~5.7). These pictures represent the behavior observed in the (*A*) 20°C–40°C, (*B*) 40°C–70°C, and (*C*) ≥70°C temperature range regimes. The different domains observed at the gel/fluid coexistence region are indicated by white arrows (*orange*/*red* areas: gel; *greenish*: fluid). The GP histograms reported in the figure correspond to a single area of the GP images (indicated by *white circles*). The bar corresponds to 20 μm.

expect a clear contrast using the Laurdan GP images. The even Laurdan distribution in the membrane and the low extent of water dipolar relaxation process in either gel-or solid-like phases will prevent the observation of a contrast between solid (crystalline) and gel phase domains in the GP images. Therefore the evaluation of the $DiIC_{18}$ and Laurdan GP images points to the fact that two different gel- (or solid)-like phases are present in the mixture at the skin physiological temperatures. Fig. 4 shows a summary of our results. Three main temperature regimes are observed in this mixture: a fluid-disordered phase above 70°C, a gel/fluid-disordered-like phase coexistence between 40°C and 70°C, and the coexistence of two gel- (or solid)-like phases below 40°C.

Effect of pH on the $_{HSC}$(Cer/Chol)/FFA mixture

Fig. 5 *A* shows the Laurdan GP temperature profile at different pHs obtained in cuvette experiments. A similar profile was observed at all pHs, mainly characterized by the presence of a main phase transition at ~65°C and the observed high GP values (gel-like) at skin physiological temperatures (i.e., low temperature regime below 40°C). As shown in Fig. 5 *B*, fluorescence microscopy was used to directly visualize the effect of pH on the lateral lipid organization below 40°C. At pH 5 the $_{HSC}$(Cer/Chol)/FFA mixture showed coexistence of two micrometer-sized gel (or solid) phases (Fig. 2). A homogeneous distribution of the fluorescent probe was observed at pH 7 followed by a strong destabilization of the lipid structures at pH 8 (Fig. 5 *B*). At skin physiological temperatures the peculiar modulation of the membrane's lateral structure occurs without significant changes in the overall phase state, i.e., the membrane display gel- (or solid)-like phases at all the studied pHs (Fig. 5 *A*).

Microscopic comparison between the $_{HSC}$(Cer/Chol)/FFA and the canonical bbCer/Chol/LA mixture

Fig. 6 *A* shows DSC and Laurdan GP cuvette data for the canonical lipid mixture bovine brain ceramide, cholesterol,

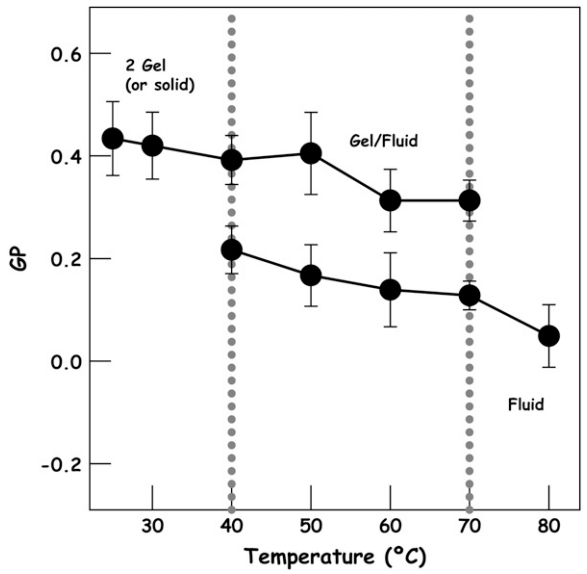

FIGURE 4 Laurdan GP average values of $_{HSC}$(Cer/Chol)/FFA at different temperatures. These values were obtained by analyzing eight different regions of each Laurdan GP image at the desired temperature. At least four different Laurdan GP images were analyzed per temperature. The dotted lines in the plot indicate the observed phase transition events in the microscopy experiments.

and lignoceric acid 1:1:1 mol ratio mixture (bbCer/Chol/LA) generally used to mimic stratum corneum membranes (68). Comparing Fig. 6 *A* with Fig. 1, some differences, but also some similarities (particularly in the DSC data; see also Table 2), are evident. Fig. 6 *B* shows the lateral structure of the bbCer/Chol/LA mixture as viewed by fluorescence microscopy. The canonical bbCer/Chol/LA mixture did form a sponge-like structure. However, the morphological characteristics of its micron-sized lipid domains differed from those of the $_{HSC}$(Cer/Chol)/FFA mixture, particularly in the low temperature (below 35°C) regime (cf. Fig. 6 *B* with Fig. 2 *B*). In this low temperature regime the commercial lipid mixture displayed up to three distinct fluorescence areas, suggesting a rather complex and different lipid lateral organization scenario with respect to that observed for the native mixture (Fig. 6 *B*). In other words the differences obtained by microscopy experiments in the low temperature regime are conclusive compared with those obtained with the other techniques (DSC and Laurdan GP in cuvette). These types of differences were also observed using another canonical skin lipid mixture composed of bovine brain ceramide, cholesterol, and palmitic acid 1:1:1 (data not shown), suggesting that the commercial skin lipid mixtures are not suitable, particularly at skin physiological temperatures, to mimic skin subcutaneous lipid membranes as previously suggested (69).

DISCUSSION AND CONCLUSIONS

Here we show that it is possible to prepare giant lipid structures from extracted human stratum corneum very long chain saturated ceramide/cholesterol/FFA mixtures. The electroformation protocol has, to our knowledge, not previously been used for mixtures devoid of phospholipids. Our skin barrier lipid model system is well suited for visualization of lipid domain coexistence in a broad temperature range (including physiological skin temperatures (25°C–35°C)) using confocal and two-photon excitation fluorescence microscopy.

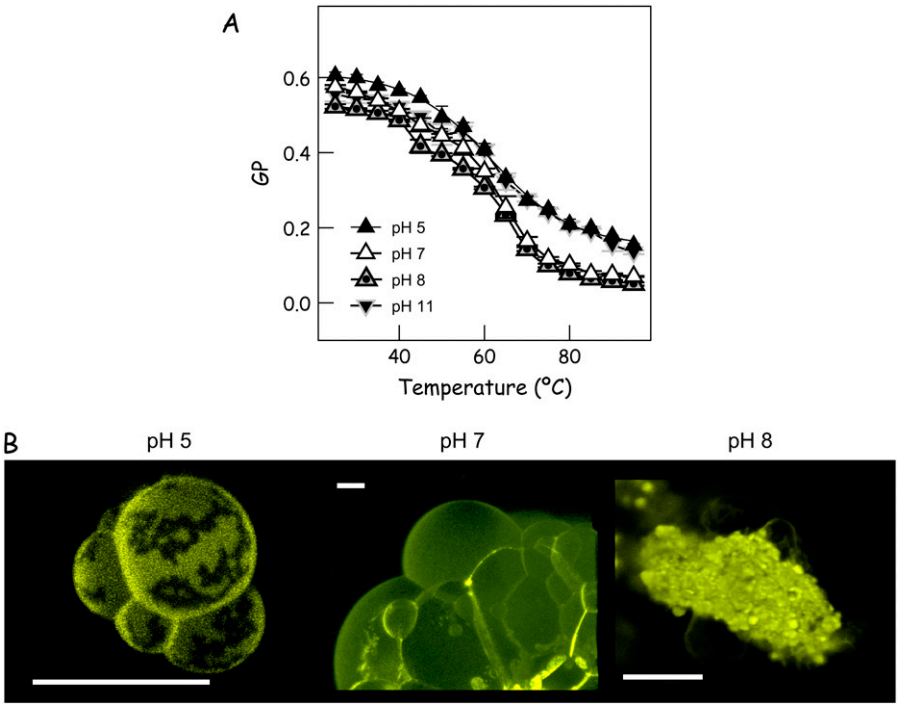

FIGURE 5 pH effect in the $_{HSC}$(Cer/Chol)/FFA lipid membranes. (*A*) Laurdan GP versus temperature of independent samples prepared with $_{HSC}$(Cer/Chol)/FFA at different pH values (see Materials and Methods). (*B*) Confocal microscopy images of DiI_{C18} labeled $_{HSC}$(Cer/Chol)/FFA membranes at different pH values. Bar is 20μm.

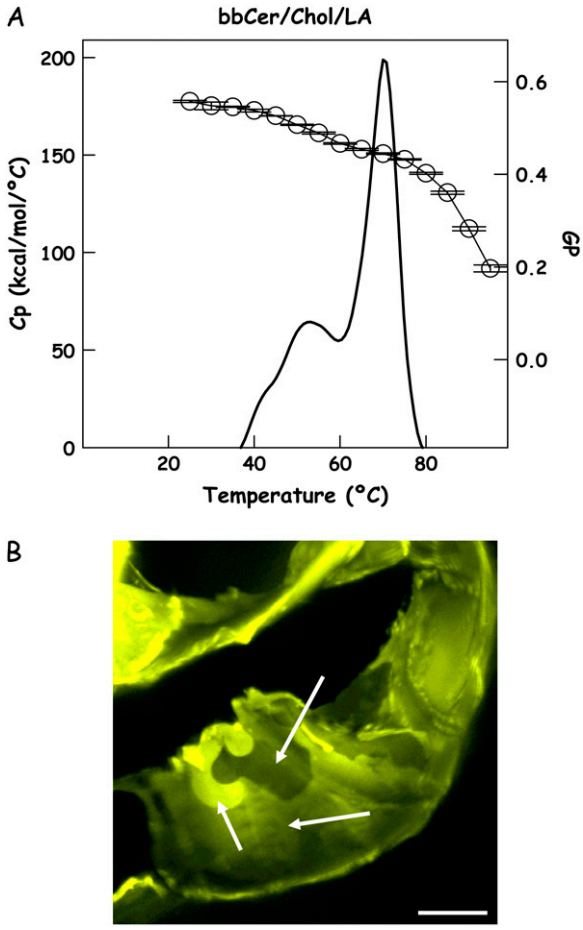

FIGURE 6 (*A*) DSC experiments and Laurdan GP temperature profile of bbCer/Chol/LA (1:1:1 mol). Two independent batches were used for this mixture. Four DSC scans and five GP measurements per temperature were performed per batch. (*B*) Confocal fluorescence 3D images (false color representation) of the bbCer/Chol/FFA in MilliQ water (pH ~5.7). The images show the observed three different fluorescent areas (indicated by *white arrows*) at 25°C. Bars are 20 μm. The fluorescent probe used was DiI_{C18}. All measurements have been repeated at least twice from independent preparations.

Lateral structure of $_{HSC}$(Cer/Chol)/FFA mixtures

The information about the thermotropic behavior of stratum corneum lipids is vast, with some differences in the main transition temperatures observed in native stratum corneum and stratum corneum lipid extracts. For example, using DSC on the integral human stratum corneum, Van Duzee observed four different thermal events at 40°C, 75°C, 85°C, and 107°C, where the phase transitions observed at 40°C and 75°C were attributed to lipid melting (57). Additionally, when the lipid components were extracted from the stratum corneum, a single phase transition at 90°C was reported in this work (57). In similar experiments, Golden et al. reported for human stratum corneum four transitions occurring at 35°C, 65°C, 80°C, and 95°C (56). Also, extraction of lipids from stratum corneum resulted in a single peak at 65°C (56), differing with the 90°C thermal event reported by Van Duzee (57). Additionally, Gay et al. (58) analyzed by means of IR spectroscopy the presence of a low thermal transition below 65°C in human stratum corneum and stratum corneum lipid extracts. These authors described two lipid phase transitions in the native stratum corneum below 65°C: one at 55°C that may reflect a complex change in the lattice structure of certain lipids and another at 35°C that may reflect a solid to fluid phase change for a small subset of human stratum corneum lipids (58). The lower temperature phase transition event (at 35°C) has been attributed to contamination of sebum lipids (56). However, Gay et al. demonstrated that the addition of an excess amount of sebum lipids to the integral stratum corneum did not affect this transition (56,58,59). Further, the stratum corneum lipid extracts showed absence of the low temperature phase transition (at 35°C) described for the intact stratum corneum (58).

The previously reported thermal event that occurs around 65°C in stratum corneum and stratum corneum lipid mixtures is evident in our experiments. This event was reported to correspond to a fluid to gel phase transition (56,58,70). However, our microscopy images (Laurdan and DiIC18) show that this event corresponds to a transition from a fluid-disordered phase to a gel/fluid-disordered phase coexistence scenario. In other words, $_{HSC}$(Cer/Chol)/FFA lipid mixture shows a broad gel/fluid-disordered phase coexistence region between 40°C and 70°C characterized by the presence of micron-sized gel domains coexisting with fluid-disordered-like lipid phases (Figs. 2 and 3). On the other hand, and in contrast to previously reported results (56–58), we observed a low-temperature main phase transition event (at ~35°C) in the $_{HSC}$(Cer/Chol)/FFA lipid mixture, using DSC and fluorescence microscopy. This event corresponds very well with that reported at similar temperatures in native human stratum corneum (for a review, see Babita et al. (59)). The observed low temperature main transition (at ~35°C) is close to skin physiological temperatures (28°C–32°C) (71) and we believe that it may have major implications for skin barrier function at physiological conditions (for a review, see Babita et al. (59)). Our results further show that the phase coexistence scenario for the $_{HSC}$(Cer/Chol)/FFA mixture in the low temperature regime (near 35°C) corresponds to the coexistence of two gel- or solid-like phases.

Absence of fluid phases in $_{HSC}$(Cer/Chol)/FFA mixtures at skin physiological temperatures

Two important observations from our experiments allowed us to conclude the absence of fluid-like phases in the $_{HSC}$(Cer/Chol)/FFA mixture at skin physiological temperatures: i) the dynamical information obtained from the Laurdan probe-associating membrane solvent dipolar relaxation with membrane lateral structure, and ii) the lipid domain information obtained by the use of $DiIC_{18}$. Even though it is clear that the Laurdan GP values obtained in the images and in the

cuvette experiments preclude the presence of a fluid-disordered phase in the low temperature regime, it is fair to consider the possibility that a fluid-ordered phase may occur in the mixture in the low temperature regime. Particularly, the presence of cholesterol in the skin mixture may cause the formation of a fluid-ordered phase. If that is the case, particularly at low temperatures, one may argue that the Laurdan GP values may not be sensitive enough to discriminate fluid-ordered-like phases from gel- or solid-like phases, because the dipolar relaxation process may be slow in both phases. This phenomenon was previously discussed by Fidorra et al. (55), who demonstrated coexistence of fluid-ordered and gel phases in POPC (1-palmitoyl-2-oleoyl-*sn*-glycero-3-phosphocholine)/ceramide/cholesterol samples (at 20 mol % of cholesterol) by means of the photoselection effect on the Laurdan probe on Laurdan GP images (55). In Fidorra et al.'s article, the Laurdan GP values of the lipid mixtures with 20 mol % of cholesterol are similar for the fluid-ordered and gel lipid phases.

However, by analyzing the photoselection effect on the Laurdan probe in these particular membranes, discrimination between fluid-ordered and gel phases was obtained (55). The photoselection effect arises from the fact that only those fluorophores which have electronic (absorption) transition moments aligned parallel or nearly so to the plane of polarization of the excitation light are excited, i.e., the excitation efficiency is proportional to the cosine squared of the angle between the electronic transition moment of the probe and the polarization plane of the excitation light. Considering a quasicircularly polarized excitation light confined in the *x*-*y* plane (as we used in our experiments), exploring different regions of the lipid structure (at a given vertical section) allows observation of different excitation efficiencies depending i) on the position of the probe's electronic transition moment relative to the plane of excitation light polarization, and ii) the lipid phase present in the membrane. An important fact here is that Laurdan transition moment is aligned parallel to the lipid chains in lipid bilayers. For example, in the walls of the sponge-like lipid structures the probe's electronic transition moment is always parallel to the polarization plane and all Laurdan molecules present in the same plane of this lipid structure will be excited with the same efficiency, i.e., regardless of the lipid phase scenario present in the vesicle (the photoselection effect does not operate; see Fig. 7 *B*).

This last fact allows calculation of the GP images without the influence of the photoselection effect (as seen in Fig. 3). On the other hand, when the membrane plane is parallel to the polarization plane of the excitation light (the probe's electronic transition moment is perpendicular to the excitation light polarization plane; Fig. 7 *A*), only fluorescence coming from the fluid-like phases (fluid ordered or fluid disordered) will be observed (66). This last selection is because

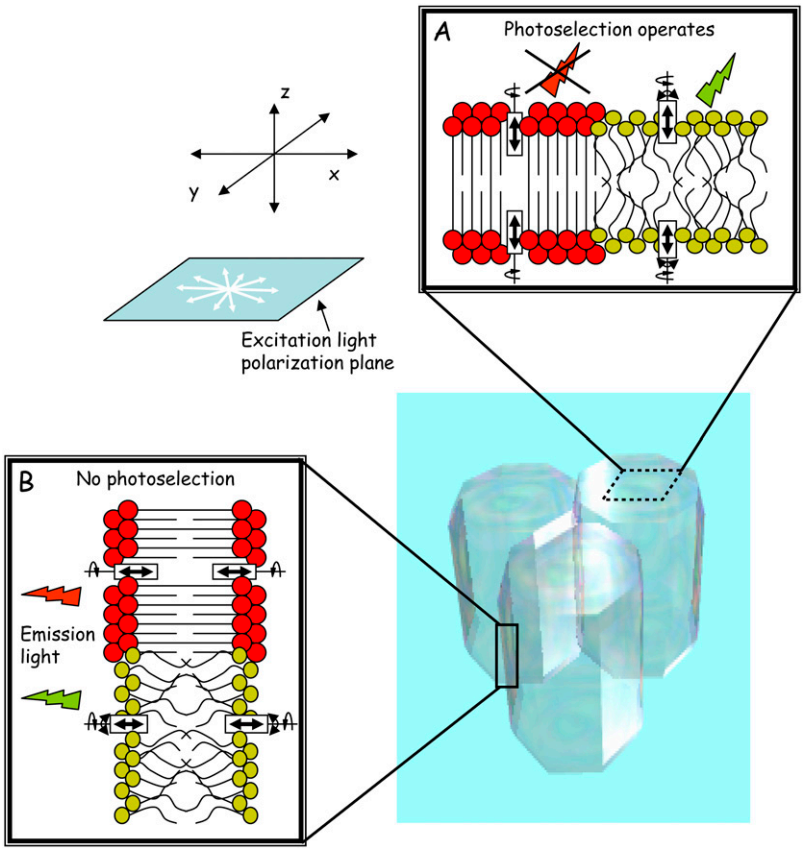

FIGURE 7 The photoselection effect in the sponge-like structures is dictated by the relative orientation of the Laurdan electronic transition moment with respect to the polarization plane of the excitation light (see text in the Discussion and Conclusions Section). A photoselection effect is observed in the membranes oriented parallel to the polarization plane (*black dotted border parallelepiped*). This effect does not operate in the wall of the sponge-like structure (*black solid border rectangle*).

a component of Laurdan's electronic transition moment is always parallel to the excitation polarization plane because of the relatively low lipid order in the fluid phases compared with the gel or solid phases (i.e., the wobbling movement of Laurdan molecules is present in fluid-like phases; Fig. 7 *A*; see Dietrich et al. (66) for more details). In our Laurdan experiments performed at the low temperature regime, no signal was observed from the membrane's regions oriented parallel to the polarization plane (where the Laurdan transition moment is perpendicular to the excitation light's polarization plane), indicating a strong photoselection effect. The last fact strongly indicates an absence of fluid-like (ordered or disordered) phases in the membrane. Additionally, the presence of two types of domains observed with $DiIC_{18}$ in the low temperature regime also supports the idea that gel- (or solid)-like phase coexistence is present.

A similar situation was reported previously for a DPPE (1,2-bis(diphenylphosphino)ethane)/DPPC (1,2 dihexadecanoyl-*sn*-glycerol-3-phosphocholine) mixture where coexistence of two different gel phases are present in the membrane at temperatures below the solidus line of the mixture's phase diagram (63). Also in this last case, the GP values for the two phases were indistinguishable and the partition of the rhodamine-phycoerythrin probe was crucial to determine the presence of the two coexisting gel phases (63). The fact that two gel- (hexagonal) or solid-like lipid phases coexist in the skin lipid mixture below 40°C can be linked with that proposed earlier (23,72) where a transition from an orthorhombic (solid) phase to a hexagonal gel phase may occur in the stratum corneum around 35°C. However, low-hydrated orthorhombic lipid phases (e.g., of fat) usually melt directly into the liquid state when heated (the melting point of orthorhombic phases being higher than that of corresponding hexagonal phases) and not via a hexagonal phase (30,31), a fact taken advantage of by the food industry in today's standard procedure for butter churning (''The Alnarp process'') (31). The coexistence of two gel phases may therefore seem more likely in the low-hydrated stratum corneum extracellular space.

The fact that fluid phases are absent in the $_{HSC}$(Cer/Chol)/FFA mixture at skin physiological temperatures contrasts with the data by Gay et al. (58), who proposed that the 35°C phase transition observed in stratum corneum corresponds to a solid to fluid phase transition type. The absence of fluid phases in the low temperature regime (below 40°C) also challenges the ''trilayer model'', which postulates the presence of a fluid phase in stratum corneum lipid membranes (73). This model, also called the ''sandwich model'', proposes that the stratum corneum lipid membranes consist of one narrow central lipid layer with fluid domains on both sides of a broad layer with a crystalline (gel-like) structure (73). It is fair to comment that if a trilayer structure is present in our membranes the fluorescent probes may be positioned in the outer layers of this particular membrane. In this last case, one can argue that the probes will not be able to sense the central (fluid) lipid layer. However, this last possibility is ruled out by the fact that the gel-like lipid domains in the giant structures composed of natural skin lipids span the entire membrane. We reasoned that the presence of fluid domains in such an arrangement will compromise the occurrence of the intralayer-coupling phenomenon (epitactic coupling (74)) observed in our images by decoupling the lipid layers. The presence of uncoupled domains was not observed in our experiments.

Effect of pH on the lateral structure of $_{HSC}$(Cer/Chol)/FFA mixtures

At pH 5 the $_{HSC}$(Cer/Chol)/FFA mixture showed the coexistence of two micrometer-sized lipid domains, whereas a homogeneous distribution of the fluorescent probe was observed at pH 7 (Fig. 5 *B*). The overall phase state of the membrane remained unchanged. Although no domain segregation was observed above pH 7, coexistence of two gel (or solid) lipid phases with nanometer-scale domain sizes (our microscopy setup has a radial resolution of ~300 nm) cannot be excluded. Which lipid species may then be involved in this pH-dependent domain size regulation? The obvious candidates are FFAs due to a pH-induced change in their ionization state. The overall pK_a of fatty acids in model stratum corneum membranes has been reported to be 6.3 (75). Deprotonation of fatty acids may strongly affect lipid-lipid interactions affecting, for instance, the line tension of the lipid domains. This effect may also be responsible for the strong membrane destabilization observed at pH 8.

The presence of lipid domains in stratum corneum is an interesting phenomenon that may be related to the permeability properties of the skin. In particular, one may think of the connection between the presence of domain boundaries and permeability events. Structural defects at the domain boundaries are likely to act as active regions where leakage of substances may happen (76,77). In addition, the observed strong pH regulation in the presence of active interfaces (the domain boundaries in this case) may suggest an additional and interesting possibility about a potential pH-dependent regulation of the skin SC permeability. It is known that a pH gradient occurs through the epidermis from the inner to outer layers (pH 7.5 to pH 4.5) (48,49). Recently using two-photon fluorescence lifetime imaging, Hanson et al. (49) showed that the stratum corneum acidic pH results from the presence of acidic aqueous pockets (average pH 6, 1 μm in diameter) within the lipid-rich extracellular matrix. This information is important not just because the lipid membranes are located in the stratum corneum extracellular matrix, but also because the average pH of the acidic pockets corresponds to the pH range where we observed a strong modulation of the lipid domain size. Permeability experiments using microscopy techniques (78) are presently performed in our laboratory to directly evaluate the effect of pH on skin membrane barrier capacity.

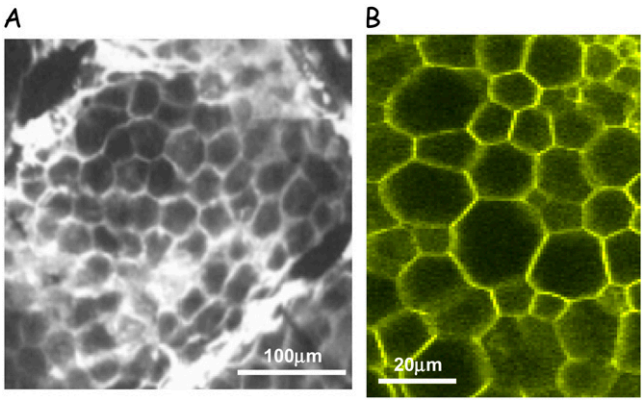

FIGURE 8 (*A*) Correlation between the structure of native stratum corneum (adapted from Simonetti et al. (79)) and (*B*) our lipid model system $_{HSC}$(Cer/Chol)/FFA. The size of keratinocytes in the stratum corneum is ~30 μm (80) in close agreement with the size distribution observed in the lipid model system (the size of the cell unit is 20.6 μm ± 4.9).

Membrane sponge-like morphology and stratum corneum cell shape

There are structural similarities between the sponge-like structure observed in our model system and the 3D structure observed in the stratum corneum (Fig. 8). Cross section images obtained in our model mixture reveals units showing a polygonal geometry with a size distribution (~30 μm) similar to that observed for lipid membranes in stratum corneum (Fig. 8). This similarity implies that extracellular lipids may affect the global 3D structure of stratum corneum cell shape and not vice versa. The possibility that stratum corneum cell shape could be independent of proteins was suggested previously by McIntosh et al. (69).

The lateral organization of the $_{HSC}$(Cer/Chol)/FFA mixture differs from that of the canonical bbCer/Chol/LA mixture

Although the canonical bbCer/Chol/LA mixture did form a giant sponge-like structure, the morphological characteristics of its micron-sized lipid domains differed from those of the $_{HSC}$(Cer/Chol)/FFA mixture. This was particularly so in the low temperature (below 35°C) regime (cf. Fig. 6 *B* with Fig. 2 *B*) where it expressed three different coexisting domains (Fig. 6 *B*). As previously proposed (69), the canonical bbCer/Chol/LA mixture should therefore be used with caution for the study of stratum corneum membrane organization and permeability.

We thank Lars Duelund for the assistance with the DSC experiments. The authors also thank Dr. David Jameson for the critical reading of the manuscript.

Research in the laboratory of L.A.B. is funded by a grant from Statens Naturvidenskabelige Forskningsråd, Denmark (21-03-0569) and the Danish National Research Foundation (which supports the MEMPHYS-Center for Biomembrane Physics). Research in the laboratory of L.N. is funded by the WennerGren Foundation, the Welander and Finsen Foundation, and the Swedish Psoriasis Foundation.

REFERENCES

1. Blank, I. H. 1952. Factors which influence the water content of the stratum corneum. *J. Invest. Dermatol.* 18:433–440.
2. Forslind, B. 1994. A domain mosaic model of the skin barrier. *Acta Derm. Venereol.* 74:1–6.
3. Michaels, A. S., S. K. Chandrasekaran, and J. E. Shaw. 1975. Drug permeation through human skin: theory and in vitro experimental measurements. *AIChE J.* 21:985–996.
4. Norlén, L. 2001. Skin barrier structure and function: the single gel phase model. *J. Invest. Dermatol.* 117:830–836.
5. Norlén, L., A. Al-Amoudi, and J. Dubochet. 2003. A cryotransmission electron microscopy study of skin barrier formation. *J. Invest. Dermatol.* 120:555–560.
6. Bouwstra, J. A., F. E. Dubbelaar, G. S. Gooris, and M. Ponec. 2000. The lipid organisation in the skin barrier. *Acta Derm. Venereol. Suppl. (Stockh.).* 208:23–30.
7. McIntosh, T. J. 2003. Organization of skin stratum corneum extracellular lamellae: diffraction evidence for asymmetric distribution of cholesterol. *Biophys. J.* 85:1675–1681.
8. Bouwstra, J. A., G. S. Pilgram, and M. Ponec. 2002. Does the single gel phase exist in stratum corneum? *J. Invest. Dermatol.* 118:897–898; author reply 899–901.
9. Norlén, L. 2002. Does the single gel phase exist in stratum corneum? Reply. *J. Invest. Dermatol.* 118:897–898; author reply 899–901.
10. Norlén, L., I. Plasencia, A. Simonsen, and P. Descouts. 2007. Human stratum corneum lipid organization as observed by atomic force microscopy on Langmuir-Blodgett films. *J. Struct. Biol.* 158:386–400.
11. Wertz, P. W., and B. B. Michniak. 2000. Sebum. *In* Cosmeceuticals: Drugs vs. Cosmetics. P. Elsner and H. I. Maibach, editors. Marcel Dekker, New York. 45–46.
12. Norlén, L., I. Nicander, A. Lundsjo, T. Cronholm, and B. Forslind. 1998. A new HPLC-based method for the quantitative analysis of inner stratum corneum lipids with special reference to the free fatty acid fraction. *Arch. Dermatol. Res.* 290:508–516.
13. Wertz, P., and L. Norlén. 2003. ''Confidence intervals'' for the ''true'' lipid composition of the human skin barrier? *In* Skin, Hair, and Nails. Structure and Function. B. Forslind and M. Lindberg, editors. Marcel Dekker. 85–106.
14. Wertz, P. W., D. C. Swartzendruber, K. C. Madison, and D. T. Downing. 1987. Composition and morphology of epidermal cyst lipids. *J. Invest. Dermatol.* 89:419–425.
15. Farwanah, H., J. Wohlrab, R. H. Neubert, and K. Raith. 2005. Profiling of human stratum corneum ceramides by means of normal phase LC/APCI-MS. *Anal. Bioanal. Chem.* 383:632–637.
16. Vietzke, J. P., O. Brandt, D. Abeck, C. Rapp, M. Strassner, V. Schreiner, and U. Hintze. 2001. Comparative investigation of human stratum corneum ceramides. *Lipids.* 36:299–304.
17. Norlén, L., I. Nicander, B. Lundh Rozell, S. Ollmar, and B. Forslind. 1999a. Inter- and intra-individual differences in human stratum corneum lipid content related to physical parameters of skin barrier function in vivo. *J. Invest. Dermatol.* 112:72–77.
18. Bouwstra, J., G. S. Gooris, M. A. Salmon-de-Vries, J. van der Spek, and W. Bras. 1992. Structure of human stratum corneum as a function of temperature and hydration: a wide-angle x-ray diffraction study. *Inter. J. Pharmaceut.* 84:205–216.
19. Garson, J. C., J. Doucet, J. L. Leveque, and G. Tsoucaris. 1991. Oriented structure in human stratum corneum revealed by x-ray diffraction. *J. Invest. Dermatol.* 96:43–49.
20. Goldsmith, L. A., and H. P. Baden. 1970. Uniquely oriented epidermal lipid. *Nature.* 225:1052–1053.
21. Hatta, I., N. Ohta, K. Inoue, and N. Yagi. 2006. Coexistence of two domains in intercellular lipid matrix of stratum corneum. *Biochim. Biophys. Acta.* 1758:1830–1836.
22. Swanbeck, G. 1959. Macromolecular organization of epidermal keratin: an x-ray diffraction study of the horny layer from normal,

ichthyotic and psoriatic skin. *Acta Derm. Venereol. Suppl. (Stockh.).* 39(Suppl. 43):1–37.

23. White, S. H., D. Mirejovsky, and G. I. King. 1988. Structure of lamellar lipid domains and corneocyte envelopes of murine stratum corneum. An x-ray diffraction study. *Biochemistry.* 27:3725–3732.
24. Wilkes, G. L., A. L. Nguyen, and R. Wildnauer. 1973. Structure-property relations of human and neonatal rat stratum corneum. I. Thermal stability of the crystalline lipid structure as studied by x-ray diffraction and differential thermal analysis. *Biochim. Biophys. Acta.* 304:265–275.
25. Pilgram, G. S., A. M. Engelsma-van Pelt, J. A. Bouwstra, and H. K. Koerten. 1999. Electron diffraction provides new information on human stratum corneum lipid organization studied in relation to depth and temperature. *J. Invest. Dermatol.* 113:403–409.
26. Bouwstra, J. A., G. S. Gooris, J. A. van der Spek, and W. Bras. 1991. Structural investigations of human stratum corneum by small-angle x-ray scattering. *J. Invest. Dermatol.* 97:1005–1012.
27. Swartzendruber, D. C., P. W. Wertz, D. J. Kitko, K. C. Madison, and D. T. Downing. 1989. Molecular models of the intercellular lipid lamellae in mammalian stratum corneum. *J. Invest. Dermatol.* 92: 251–257.
28. Al-Amoudi, A., J. Dubochet, and L. Norlén. 2005. Nanostructure of the epidermal extracellular space as observed by cryo-electron microscopy of vitreous sections of human skin. *J. Invest. Dermatol.* 124:764–777.
29. Charalambopoulos, G. C., T. A. Striotis, T. Hauss, A. K. Stubos, and N. K. Kanellopoulos. 2004. Structural alterations of fully hydrated human stratum corneum. *Physica B (Amsterdam).* 350:e603–e606.
30. Hernquist, L. 1984. Polymorphism of fats. PhD thesis. Lund University, Lund, Sweden.
31. Larsson, K. 1994. Lipids: molecular organisation, physical functions and technical applications. The Oily Press, Dundee, Scotland.
32. Carruthers, A., and D. L. Melchior. 1983. Studies of the relationship between bilayer water permeability and bilayer physical state. *Biochemistry.* 22:5797–5807.
33. Naik, A., and R. H. Guy. 1997. Infrared spectroscopy and differential scanning calorimetric investigations of the stratum corneum barrier function. *In* Mechanisms of Transdermal Drug Delivery. R. O. Potts and R. H. Guy, editors. Marcel Dekker, New York. 87–162.
34. Ananthapadmanabhan, K. P., A. Lips, C. Vincent, F. Meyer, C. Caso, A. Johnson, K. Subramanyan, M. Vetharmuthu, G. Rattinger, and D. J. Moore. 2003. pH-induced alterations in stratum corneum properties. *Int. J. Cosm. Sci.* 25:103–112.
35. Behne, M. J., N. P. Barry, K. M. Hanson, I. Aronchik, R. W. Clegg, E. Gratton, K. Feingold, W. M. Holleran, P. M. Elias, and T. M. Mauro. 2003. Neonatal development of the stratum corneum pH gradient: localization and mechanisms leading to emergence of optimal barrier function. *J. Invest. Dermatol.* 120:998–1006.
36. Fluhr, J. W., M. Mao-Qiang, B. E. Brown, J. P. Hachem, D. G. Moskowitz, M. Demerjian, M. Haftek, G. Serre, D. Crumrine, T. M. Mauro, P. M. Elias, and K. R. Feingold. 2004. Functional consequences of a neutral pH in neonatal rat stratum corneum. *J. Invest. Dermatol.* 123:140–151.
37. Hachem, J. P., D. Crumrine, J. Fluhr, B. E. Brown, K. R. Feingold, and P. M. Elias. 2003. pH directly regulates epidermal permeability barrier homeostasis, and stratum corneum integrity/cohesion. *J. Invest. Dermatol.* 121:345–353.
38. Hachem, J. P., M. Q. Man, D. Crumrine, Y. Uchida, B. E. Brown, V. Rogiers, D. Roseeuw, K. R. Feingold, and P. M. Elias. 2005. Sustained serine proteases activity by prolonged increase in pH leads to degradation of lipid processing enzymes and profound alterations of barrier function and stratum corneum integrity. *J. Invest. Dermatol.* 125:510–520.
39. Eberlein-Konig, B., T. Schafer, J. Huss-Marp, U. Darsow, M. Mohrenschlager, O. Herbert, D. Abeck, U. Kramer, H. Behrendt, and J. Ring. 2000. Skin surface pH, stratum corneum hydration, transepidermal water loss and skin roughness related to atopic eczema and skin dryness in a population of primary school children. *Acta Derm. Venereol.* 80:188–191.
40. Öhman, H., and A. Vahlquist. 1998. The pH gradient over the stratum corneum differs in X-linked recessive and autosomal dominant ichthyosis: a clue to the molecular origin of the ''acid skin mantle''? *J. Invest. Dermatol.* 111:674–677.
41. Schmid-Wendtner, M. H., and H. C. Korting. 2006. The pH of the skin surface and its impact on the barrier function. *Skin Pharmacol. Physiol.* 19:296–302.
42. Werner, Y., and M. Lindberg. 1985. Transepidermal water loss in dry and clinically normal skin in patients with atopic dermatitis. *Acta Derm. Venereol.* 65:102–105.
43. Cunico, R. L., H. I. Maibach, H. Khan, and E. Bloom. 1977. Skin barrier properties in the newborn. Transepidermal water loss and carbon dioxide emission rates. *Biol. Neonate.* 32:177–182.
44. Berg, R. W., M. C. Milligan, and F. C. Sarbaugh. 1994. Association of skin wetness and pH with diaper dermatitis. *Pediatr. Dermatol.* 11: 18–20.
45. Nilsson, G. E. 1977. On the measurements of evaporative water loss—methods and clinical applications. PhD thesis. Dept. of Medical Engineering, University of Linköping, Linköping, Sweden.
46. Norlén, L., J. Engblom, M. Andersson, and B. Forslind. 1999. A new computer-based evaporimeter system for rapid and precise measurements of water diffusion through stratum corneum in vitro. *J. Invest. Dermatol.* 113:533–540.
47. Denda, M., J. Hosoi, and Y. Asida. 2000. Visual imaging of ion distribution in human epidermis. *Biochem. Biophys. Res. Commun.* 272: 134–137.
48. Öhman, H., and A. Vahlquist. 1994. In vivo studies concerning a pH gradient in human stratum corneum and upper epidermis. *Acta Derm. Venereol.* 74:375–379.
49. Hanson, K. M., M. J. Behne, N. P. Barry, T. M. Mauro, E. Gratton, and R. M. Clegg. 2002. Two-photon fluorescence lifetime imaging of the skin stratum corneum pH gradient. *Biophys. J.* 83:1682–1690.
50. Ouimet, J., S. Croft, C. Pare, J. Katsaras, and M. Lafleur. 2003. Modulation of the polymorphism of the palmitic acid/cholesterol system by the pH. *Langmuir.* 19:1089–1097.
51. Keller, D., N. B. Larsen, I. M. Moller, and O. G. Mouritsen. 2005. Decoupled phase transitions and grain-boundary melting in supported phospholipid bilayers. *Phys. Rev. Lett.* 94:025701.
52. Bouwstra, J. A., G. S. Gooris, F. E. Dubbelaar, A. M. Weerheim, and M. Ponec. 1998. pH, cholesterol sulfate, and fatty acids affect the stratum corneum lipid organization. *J. Investig. Dermatol. Symp. Proc.* 3:69–74.
53. Bagatolli, L. A. 2006. To see or not to see: lateral organization of biological membranes and fluorescence microscopy. *Biochim. Biophys. Acta.* 1758:1541–1556.
54. Parasassi, T., G. De Stasio, A. d'Ubaldo, and E. Gratton. 1990. Phase fluctuation in phospholipid membranes revealed by Laurdan fluorescence. *Biophys. J.* 57:1179–1186.
55. Fidorra, M., L. Duelund, C. Leidy, A. Simonsen, and L. A. Bagatolli. 2006. Absence of fluid-ordered/fluid-disordered phase coexistence in ceramide/POPC mixtures containing cholesterol. *Biophys. J.* 90:4437–4451.
56. Golden, G. M., D. B. Guzek, R. R. Harris, J. E. McKie, and R. O. Potts. 1986. Lipid thermotropic transitions in human stratum corneum. *J. Invest. Dermatol.* 86:255–259.
57. Van Duzee, B. F. 1975. Thermal analysis of human stratum corneum. *J. Invest. Dermatol.* 65:404–408.
58. Gay, C. L., R. H. Guy, G. M. Golden, V. H. Mak, and M. L. Francoeur. 1994. Characterization of low-temperature (i.e., $<$ 65 degrees C) lipid transitions in human stratum corneum. *J. Invest. Dermatol.* 103: 233–239.
59. Babita, K., V. Kumar, V. Rana, S. Jain, and A. K. Tiwary. 2006. Thermotropic and spectroscopic behavior of skin: relationship with percutaneous permeation enhancement. *Curr. Drug Des. Deliv.* 3:95–113.

60. Parasassi, T., and E. Gratton. 1995. Membrane lipid domains and dynamics as detected by Laurdan fluorescence. *J. Fluoresc.* 2:167–174.

61. Bagatolli, L. A. 2003. Thermotropic behavior of lipid mixtures studied at the level of single vesicles: giant unilamellar vesicles and two-photon excitation fluorescence microscopy. *Methods Enzymol.* 367:233–253.

62. Bagatolli, L. A., and E. Gratton. 2001. Direct observation of lipid domains in freestanding bilayers using two-photon excitation fluorescence microscopy. *J. Fluoresc.* 11:141–160.

63. Bagatolli, L. A., and E. Gratton. 2000. A correlation between lipid domain shape and binary phospholipid mixture composition in free standing bilayers: a two-photon fluorescence microscopy study. *Biophys. J.* 79:434–447.

64. Mathivet, L., S. Cribier, and P. F. Devaux. 1996. Shape change and physical properties of giant phospholipid vesicles prepared in the presence of an AC electric field. *Biophys. J.* 70:1112–1121.

65. Bernardino de la Serna, J., J. Perez-Gil, A. C. Simonsen, and L. A. Bagatolli. 2004. Cholesterol rules: direct observation of the coexistence of two fluid phases in native pulmonary surfactant membranes at physiological temperatures. J. Biol. Chem. 279:40715–40722.

66. Dietrich, C., L. A. Bagatolli, Z. N. Volovyk, N. L. Thompson, M. Levi, K. Jacobson, and E. Gratton. 2001. Lipid rafts reconstituted in model membranes. *Biophys. J.* 80:1417–1428.

67. Saenz, A., O. Canadas, L. A. Bagatolli, M. E. Johnson, and C. Casals. 2006. Physical properties and surface activity of surfactant-like membranes containing the cationic and hydrophobic peptide KL. *FEBS J.* 273:2515–2527.

68. ten Grotenhuis, E., R. A. Demel, M. Ponec, D. R. Boer, J. C. van Miltenburg, and J. A. Bouwstra. 1996. Phase behavior of stratum corneum lipids in mixed Langmuir-Blodgett monolayers. *Biophys. J.* 71:1389–1399.

69. McIntosh, T. J., M. E. Stewart, and D. T. Downing. 1996. X-ray diffraction analysis of isolated skin lipids: reconstitution of intercellular lipid domains. *Biochemistry.* 35:3649–3653.

70. Gooris, G. S., and J. A. Bouwstra. 2007. Infrared spectroscopic study of stratum corneum model membranes prepared from human ceramides, cholesterol, and fatty acids. *Biophys. J.*92:2785–2795.

71. Glombitza, B., and C. C. Muller-Goymann. 2002. Influence of different ceramides on the structure of in vitro model lipid systems of the stratum corneum lipid matrix. *Chem. Phys. Lipids.* 117: 29–44.

72. Bouwstra, J. A., and M. Ponec. 2006. The skin barrier in healthy and diseased state. *Biochim. Biophys. Acta.* 1758:2080–2095.

73. Bouwstra, J. A., P. L. Honeywell-Nguyen, G. S. Gooris, and M. Ponec. 2003. Structure of the skin barrier and its modulation by vesicular formulations. *Prog. Lipid Res.* 42:1–36.

74. Merkel, R., E. Sackmann, and E. Evans. 1989. Molecular friction and epitactic coupling between monolayers in supported bilayers. *J. Phys. France.* 50:1535–1555.

75. Lieckfeldt, R., J. Villalain, J. C. Gomez-Fernandez, and G. Lee. 1995. Apparent pK_a of the fatty acids within ordered mixtures of model human stratum corneum lipids. *Pharm. Res.* 12:1614–1617.

76. Montes, L. R., M. B. Ruiz-Arguello, F. M. Goni, and A. Alonso. 2002. Membrane restructuring via ceramide results in enhanced solute efflux. *J. Biol. Chem.* 277:11788–11794.

77. Papahadjopoulos, D., K. Jacobson, S. Nir, and T. Isac. 1973. Phase transitions in phospholipid vesicles. Fluorescence polarization and permeability measurements concerning the effect of temperature and cholesterol. *Biochim. Biophys. Acta.* 311:330–348.

78. Ambroggio, E. E., F. Separovic, J. H. Bowie, G. D. Fidelio, and L. A. Bagatolli. 2005. Direct visualization of membrane leakage induced by the antibiotic peptides: maculatin, citropin, and aurein. *Biophys. J.* 89:1874–1881.

79. Simonetti, O., A. J. Hoogstraate, W. Bialik, J. A. Kempenaar, A. H. Schrijvers, H. E. Bodde, and M. Ponec. 1995. Visualization of diffusion pathways across the stratum corneum of native and in-vitro-reconstructed epidermis by confocal laser scanning microscopy. *Arch. Dermatol. Res.* 287:465–473.

80. Forslind, B. 1995. The skin: upholder of physiological homeostasis. A physiological and (bio) physical study program. *Thromb. Res.* 80:1–22.